Adsorption and Reaction of SO_2 on Model $Ce_{1-x}Zr_xO_2(111)$ Catalysts

Gang Liu, José A. Rodriguez,* Zhipeng Chang, and Jan Hrbek

Chemistry Department, Brookhaven National Laboratory, Upton, New York 11953

Charles H. F. Peden

Chemical Sciences Division, Pacific Northwest National Laboratory, Richland, Washington 99352

Received: June 30, 2003; In Final Form: December 16, 2003

The interaction of SO_2 with ceria−zirconia model catalysts was studied using high-resolution synchrotron-based X-ray photoelectron spectroscopy (XPS). Epitaxial $Ce_{1-x}Zr_xO_2(111)$ ($x = 0.1$ and 0.3) thin films (500−700 Å in thickness) were grown by oxygen-plasma-assisted molecular beam epitaxy on single-crystal Y-stabilized $ZrO_2(111)$. Slightly defective surfaces were achieved by vacuum annealing at 900 K, and highly defective surfaces with O vacancies were obtained by 1.5-keV Ne^+ sputtering. On the slightly defective $Ce_{0.9}Zr_{0.1}O_{1.95}(111)$ and $Ce_{0.7}Zr_{0.3}O_{1.95}(111)$ surfaces, the only products upon SO_2 adsorption at 300 K are SO_4/SO_3 species, which gradually desorb from the surface between 300 and 900 K. SO_2 adsorption on the heavily reduced surfaces results in different behavior. A complex set of compounds is observed during adsorption and thermal conversion processes. The $Ce^{\delta+}$ states ($\delta \leq 3$) play a dominant role in the adsorption of SO_2 and cleavage of S−O bonds. The relative amount of sulfur-derived adsorbates depends on the defect concentration: the higher the $Ce^{\delta+}$ concentration, the larger the amount of formed atomic S. On $Ce_{0.9}Zr_{0.1}O_{1.50}(111)$ and $Ce_{0.7}Zr_{0.3}O_{1.50}(111)$ surfaces, sulfate, sulfite, and atomic sulfur species coexist at 300 K. The Zr cations increase the stability of the SO_4/SO_3 groups on the oxide surface. Thermal annealing (for $Ce_{0.9}$ $Zr_{0.1}O_{1.50}(111)$, >400 K; for $Ce_{0.7}Zr_{0.3}O_{1.50}(111)$, >700 K) leads to the formation of oxy-sulfides (M_2O_2S, M= Ce or Zr), which are converted from either sulfate or sulfite. The formation of the oxy-sulfides produces a substantial shift in the Zr 3d core levels.

Introduction

The continuous demand for the reduction of toxic emissions from automotive engines has driven extensive research toward improving existing automotive catalysts or developing new ones for more efficient cleanup processes.[1] Ceria (CeO_2) is a crucial support and component in three-way automotive catalysts because of its ability to release or uptake oxygen under reducing or oxidizing conditions, respectively.[2−4] The facile conversion between the Ce^{4+} and Ce^{3+} oxidation states of ceria allows the automotive catalysts to operate over wider air-to-fuel ratios in the catalytic converters, in which CO, hydrocarbons, and NO_x can be removed or transformed simultaneously.[3] To enhance the redox properties and thermal resistance of pure ceria, zirconia (ZrO_2) is mixed as an additive to form solid solutions of the $Ce_{1-x}Zr_xO_2$ type. Recently, studies of zirconia doping effects have received a lot of attention.[5−9] Our recent experimental and theoretical studies[8,9] show that the presence of zirconia promotes the formation of Ce^{3+} defect states and associated nonequivalent O atoms in the $Ce_{1-x}Zr_xO_2$ ($x \leq 0.5$) compounds. Despite the extensive use of ceria−zirconia mixed oxides in advanced exhaust catalysts, the details of the complex effects of zirconia doping still remain uncertain, and more systematic studies are needed.

Here, our major concern is the chemistry of SO_2 on $Ce_{1-x}Zr_xO_2(111)$ surfaces. In the area of environmental catalysis, significant attention has been directed to the investigation of the destruction of sulfur dioxide ($DeSO_x$ process).[10−12] SO_2 is frequently generated during the burning of fossil-derived fuels in factories, power plants, and automobiles and has negative effects on catalytic activity and the environment.[12] In general, sulfur species in the form of organo-sulfur compounds are present in gasoline and other fuels. In the typical engine exhaust, 5−20 ppm of SO_2 is formed after combustion, and SO_2 poisons the ceria used in the automotive catalytic converters.[13−16] The species responsible for ceria deactivation is mainly attributed to cerium sulfate, which blocks the Ce^{3+} sites for the redox cycle in the process of oxygen storage.[14−16] Boaro et al.[16] has suggested that SO_2 deactivates the oxygen storage capacity in both ceria and ceria−zirconia compounds at temperatures lower than 973 K, and sulfates in the form of $Ce_2(SO_4)_3$ (Ce^{3+} sulfates) play a key role. In addition to studies with ceria catalysts,[15,16] a number of fundamental surface-science studies have been conducted to examine the species generated upon SO_2 adsorption.[17−19] The reaction of SO_2 with CeO_2 powders and polycrystalline films supported on Pt(111) at 300 K shows sulfate (SO_4^{2-}) as the main surface species as evidenced by a combination of X-ray absorption spectroscopy (XANES), temperature-programmed desorption (TPD), and high-resolution X-ray photoelectron spectroscopy (XPS). SO_4 decomposes in the temperature range of 390−670 K, and oxygen vacancies favor the formation of SO_3 instead of SO_4.[17] For SO_2 adsorption on polycrystalline ceria thin films supported on Mo(100), SO_3 is a primary surface species, and only a small extent of sulfate formation occurs.[18] Vacuum annealing results in additional formation of sulfate species and decomposition of sulfate to

* To whom correspondence should be addressed. E-mail: rodrigez@bnl.gov. Fax: 631-344-5815.

10.1021/jp030808g CCC: $27.50
Published on Web 02/07/2004

sulfide (Ce_2O_2S) above 823 K.[18] It has been reported that SO_3 is the main product in the adsorption of SO_2 on $CeO_2(111)$// Ru(0001),[19] but the formed SO_x species exhibits S 2p binding energies close to those of the SO_4 formed on CeO_2//Pt(111).[17] The diverse surface chemistry for SO_2 adsorption on these model catalysts could be attributed to the different synthesis procedures and supporting substrates, which govern the thin film quality and associated chemical properties of the surfaces. For example, oxygen vacancies are thought to alter the SO_2 adsorption behavior[17,18] dramatically, and their concentration in the model films could vary significantly in the published studies.[17−19]

In this study, we examined the electronic and chemical properties of $Ce_{1-x}Zr_xO_2(111)$ ($x = 0.1$ and 0.3) using synchrotron-based high-resolution photoemission. We place particular emphasis on determining how the Zr substitution of Ce at the cation sites affects the SO_2 chemistry via structural and/or electronic perturbations. We are unaware of published experimental data examining the surface chemistry of SO_2 on single-crystal ceria−zirconia mixed oxides with a variety of oxygen vacancy concentrations.

Experimental Section

The experimental work was carried out in an ultrahigh-vacuum (UHV) chamber that forms part of the U7A beamline[8] in the National Synchrotron Light Source (NSLS) at Brookhaven National Laboratory. The UHV chamber (with a base pressure of $\sim 5 \times 10^{-10}$ Torr) is fitted with a hemispherical electron energy analyzer with multichannel detection, optics for low-energy electron diffraction (LEED), a residual gas analyzer (SRS-RGA), and a twin (Mg Kα and Al Kα) X-ray source. The combined energy resolution in the synchrotron experiments was 0.3−0.4 eV. For the photoemission measurements, the binding-energy (BE) values were determined with respect to the Fermi level.

$Ce_{1-x}Zr_xO_2(111)$ ($x = 0.1$ and 0.3) thin films (500−700 Å in thickness) were grown on a Y-stabilized $ZrO_2(111)$ surface by oxygen-plasma-assisted molecular-beam epitaxy.[20,21] The pure-phase, atomically flat films were characterized by reflection high-energy electron diffraction (RHEED), LEED, XPS, X-ray photoelectron diffraction (XPD), X-ray diffraction (XRD), and Rutherford backscattering spectrometry and channeling (RBS/C). The details of growing conditions and characterizing procedures are described elsewhere.[20,21]

The oxide samples were sandwiched between Ta plates that were spot-welded to two Ta heating legs of a manipulator.[8] The samples could be cooled as low as 100 K by thermal contact with a liquid-nitrogen reservoir and resistively heated to 1200 K. The temperature was monitored by a type-C thermocouple spot-welded on the Ta plate edge.[8] Sample cleaning and treatment included annealing (∼600−700 K) in an oxygen environment (2×10^{-6} Torr), sputtering with Ne^+ ions (1 keV, 2×10^{-5} Torr), and annealing (∼700−900 K) in vacuum.[8] For the fully oxidized $Ce_{0.9}Zr_{0.1}O_2$ and $Ce_{0.7}Zr_{0.3}O_2$ surfaces, there were serious charging problems during the collection of the photoemission spectra. To avoid this, defects in the thin films were created for better electronic conductivity, with the extent of reduction controlled by either vacuum annealing up to 900 K or Ne^+ bombardment at 1.5 keV.[8] Ion sputtering removed surface O without significantly altering the Ce-to-Zr ratio as was seen in our previous study.[8] The amount of oxygen removed near the surface was estimated from the relative intensity of the O 1s peak to the Ce and Zr core-level peaks and variations in the signal for the Ce^{4+} and $Ce^{\delta+}$ ($\delta \leq 3$) states in photoemission.[8,22,23] This procedure does not measure the exact amount of O removed, but it is useful in establishing the relative concentration of O vacancies near the surface. We worked with samples that were slightly sputtered, $Ce_{1-x}Zr_xO_{1.95}(111)$ in our notation, and samples that were heavily sputtered, $Ce_{1-x}Zr_xO_{1.50}(111)$ in our notation. Not a large number of O vacancies are expected under the common conditions in which automotive catalysts operate, but a large number of O vacancies can be the key for the high activity of catalysts used for the destruction of SO_2.[2a,3,12]

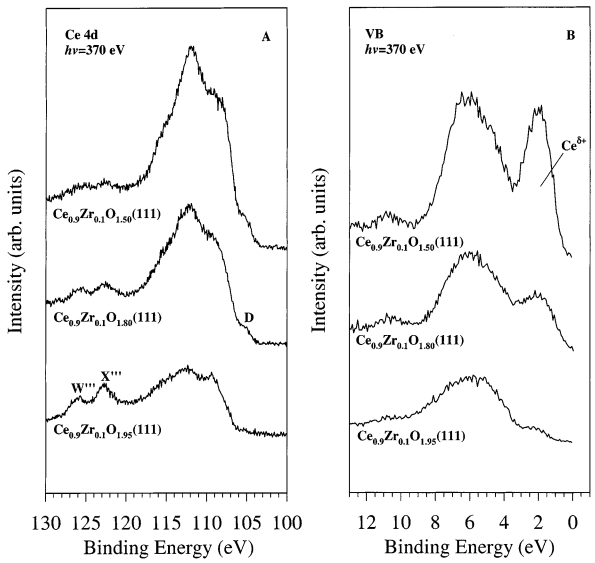

Figure 1. Ce 4d core-level spectra (left panel) and valence band spectra (right panel) for $Ce_{0.9}Zr_{0.1}O_{2-x}(111)$ with different defect populations ($\delta \leq 3$). The spectra were obtained using a photon energy of 370 eV.

The dosing of high-purity sulfur dioxide (99.98%, Mattheson) at room temperature was performed through a leak valve with a stainless tube directed to the sample surface. The SO_2 exposures (1 langmuir = 10^{-6} Torr·s) were based on the ion-gauge reading without further correction.

Results

3.1. SO_2 Interaction with $Ce_{0.9}Zr_{0.1}O_{2-x}(111)$. Figure 1 displays Ce 4d core-level and valence spectra for $Ce_{0.9}Zr_{0.1}O_{2-x}(111)$ systems with different defect populations near the surface ($x = 0.05$, 0.20, and 0.50). As mentioned in section 2, the $Ce_{0.9}Zr_{0.1}O_{1.95}(111)$ system was prepared by UHV annealing up to 900 K after full oxidation in an oxygen environment, and the $Ce_{0.9}Zr_{0.1}O_{1.80}(111)$ and $Ce_{0.9}Zr_{0.1}O_{1.50}(111)$ systems were prepared by 1.5-keV Ne^+ sputtering for 5 and 10 min, respectively. The concentration for oxygen in the surface region was estimated as described in section 2, and here we are interested only in the relative amount of oxygen removed. Following standard practice in the literature, features in the photoemission spectra will be attributed to Ce^{4+}, Ce^{3+}, Zr^{4+}, or Zr^{2+} ions. The reader should keep in mind that these are *formal* assignments and that the oxides under study are far from being fully ionic.[2b,c,8] They are best described as ionocovalent compounds or covalent insulators.[2b] Furthermore, for heavily reduced Ce−Zr oxide surfaces the core level and valence features typically assigned to Ce^{3+} can contain contributions from Ce cations in a lower oxidation state.[2,7,8]

In agreement with previous studies,[8,14b] the removal of O from the $Ce_{0.9}Zr_{0.1}O_2(111)$ system led to the formation of reduced cerium species ($Ce^{\delta+}$, $\delta \leq 3$) without a significant reduction of the Zr^{4+} cations. In Figure 1A, the Ce 4d spectra display multiple electronic features and are very sensitive to the

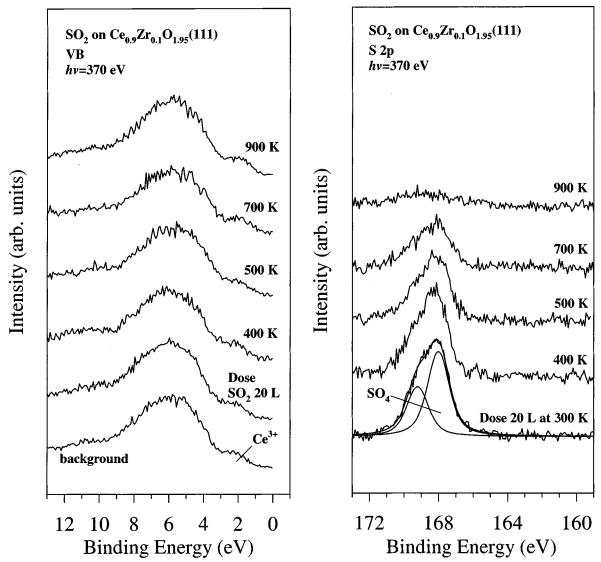

Figure 2. Effects of SO_2 adsorption and subsequent annealing on the valence band spectra (left panel, $h\nu = 370$ eV) and corresponding S 2p spectra (right panel, $h\nu = 370$ eV) of a slightly defective $Ce_{0.9}Zr_{0.1}O_{1.95}(111)$ surface.

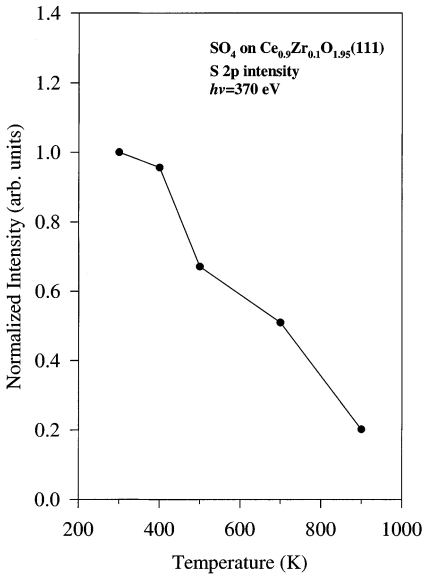

Figure 3. S 2p intensity for sulfate species (SO_4) on $Ce_{0.9}Zr_{0.1}O_{1.95}$-(111) (see Figure 2) as a function of annealing temperature.

oxidation state of the Ce cations.[22,23] Because of the suppression of charging, the overall photoemission signal increases when the number of defects is raised in the system.[8] In the present study, the peak assignments and labels W‴, X‴, and D follow the previous convention introduced by Burroughs et al.[24] and Mullins et al.[23] X‴ and W‴ peaks reflect the emission from Ce $4d_{5/2}$ and Ce $4d_{3/2}$ components, respectively, and the D state is directly related to the proportion of the Ce^{3+} component. The X‴ and W‴ doublet exhibits an energy difference of 3.3 eV, consistent with the data for pure ceria.[23] The complex structure of the spectra is due to various initial and final states.[23,24] Figure 1A shows that there are significant changes in terms of the line shape and intensity with the degree of reduction of the samples. The line shape of Ce 4d spectra for a slightly defective $Ce_{0.9}Zr_{0.1}O_{1.95}(111)$ surface is mainly derived from Ce^{4+} contributions and without D emission. With the increasing degree of reduction from $Ce_{0.9}Zr_{0.1}O_{1.95}(111)$ to $Ce_{0.9}Zr_{0.1}O_{1.50}(111)$, the intensity in the region between X‴ and D and the D peak intensity increase. The variation of the Ce 4d complex structure with the changing degree of reduction for zirconia-doped ceria is very similar to that of pure ceria,[23] suggesting the dominant role of ceria in these solid solutions. Figure 1B displays the corresponding valence band spectra. The valence band structure is mainly seen from ca. 3 to 9 eV. This feature is mainly assigned to O 2p valence orbitals.[8] For the slightly reduced $Ce_{0.9}Zr_{0.1}O_{1.95}$-(111), there is a relatively weak emission between the Fermi level and the O 2p states. Similar to that of pure ceria, the band gap state is mostly derived from Ce^{3+} cations and is related to occupied Ce $4f^1$ electronic states at a BE of ~2 eV.[8] Figure 1B shows that from $Ce_{0.9}Zr_{0.1}O_{1.95}(111)$ to $Ce_{0.9}Zr_{0.1}O_{1.50}(111)$ the population of the $Ce^{\delta+}$ states relative to the O 2p intensity is significantly increased. The changing trend of the valence band of zirconia-doped ceria is consistent with that of the Ce 4d core-level spectra. In the following part of this section, we will examine the role of the $Ce^{\delta+}$ defect states in the chemistry of SO_2 on ceria−zirconia compounds.

The left panel of Figure 2 displays the effect of SO_2 dosing and subsequent annealing on the valence features of $Ce_{0.9}Zr_{0.1}O_{1.95}(111)$. SO_2 (20 L) was dosed at 300 K followed by stepwise heating to 900 K. The exposure of 20 L was enough to reach the "saturation" coverage. Figure 2 clearly shows that SO_2 dosing and annealing does not significantly attenuate the intensity of the Ce^{3+} states for this system. (In this case, the number of O vacancies is small, and the formal oxidation state of cerium is expected not to be lower than +3.) In addition, the SO_2 adsorption does not result in an obvious partial reduction of the ceria surface. On pure ceria, SO_2 may be oxidized to sulfate (SO_4 in our notation) with a partial reduction of the ceria.[18] The right panel of Figure 2 displays photoemission S 2p core-level spectra for the adsorption of SO_2. Charging problems led to a poor signal/noise ratio in these photoemission spectra (section 2). Only one doublet appears after an exposure of 20 L of SO_2. The curve-fitting[25] results for the spectrum at 300 K reveal the existence of one sulfur species (the solid line going through the data represents the calculated total intensity), with S $2p_{1/2}$ and S $2p_{3/2}$ peaks centered at 169.2 and 168.0 eV, respectively. These BE values are in agreement with those reported in the literature for the adsorption of SO_2 on pure ceria surfaces[17−19] and can be assigned to a sulfate-type species,[17] but the existence of a sulfite-type species (SO_3 in our notation) cannot be ruled out.[19] With the increase of annealing temperature, the S 2p peak intensity progressively decreases. No significant BE shift is observed during the evolution of the S 2p peak intensity, and no other sulfur species such as oxy-sulfide (Ce_2O_2S) or atomic sulfur appears by heating to 900 K. The change in S 2p intensity with the annealing temperature is displayed in Figure 3. By 900 K, most of the SO_2-derived species disappears, and the peak intensity is only ~20% of that at 300 K. The changes in Zr 3d core-level spectra for SO_2 adsorption and desorption were also recorded (data not shown). No significant variations for either the peak positions or the line shape of the Zr $3d_{5/2}$ (~183.2 eV) and Zr $3d_{3/2}$ (~185.5 eV) components during SO_2 adsorption and subsequent annealing were seen. A slight decrease in the intensity of the Zr 3d signal upon SO_2 adsorption was simply due to attenuation by the adsorbed molecules, and this effect was essentially removed by annealing to high temperature.

The behavior of SO_2 is expected to depend on the oxidation state or the presence of defects in $Ce_{0.9}Zr_{0.1}O_2(111)$ surfaces. Figure 4 shows that the S 2p profiles for a highly defective surface are much more complex than for the almost fully oxidized surface studied above. A number of sulfur species are

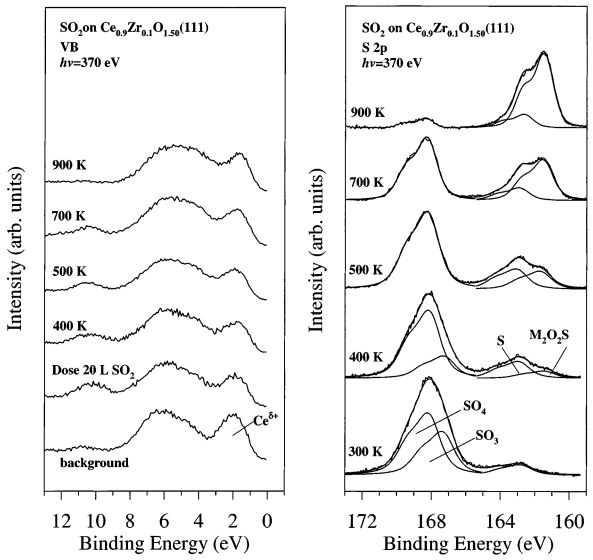

Figure 4. Effects of SO_2 adsorption and subsequent annealing on the valence band (left panel, $h\nu = 370$ eV) and S 2p spectra (right panel, $h\nu = 370$ eV) of a highly defective $Ce_{0.9}Zr_{0.1}O_{1.50}(111)$ surface containing $Ce^{\delta+}$ ($\delta \leq 3$). M = Ce or Zr.

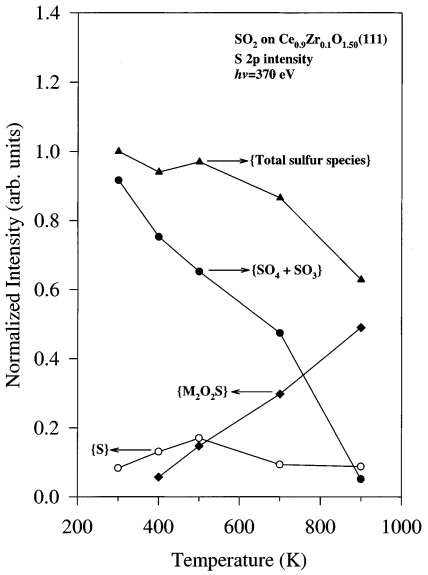

Figure 5. Change in S 2p intensity for the total concentration of sulfur species, sulfate (SO_4) plus sulfite (SO_3), atomic sulfur, and oxy-sulfides (M_2O_2S, M = Ce or Zr) on $Ce_{0.9}Zr_{0.1}O_{1.50}(111)$ (see Figure 4) as a function of annealing temperature.

observed on the surfaces, depending on the sample annealing temperatures. After we subtracted a Shirley background, the spectra were curve fit by a set of three or four doublets following the procedure described in ref 25. The solid line going through the data represents the total intensity calculated during the curve fitting. For the adsorption of SO_2 at 300 K, the S 2p spectrum showed three different types of species. The line shape implies that there are two doublets located between 166 and 171 eV, with S $2p_{3/2}$ BE appearing at 168.2 and 167.3 eV, respectively. They can be tentatively assigned to the formation of sulfate and sulfite,[17,18] but the identification of these species on the basis of only photoemission is not conclusive.[17−19] A small fraction of the adsorbed SO_2 is decomposed into an atomic sulfur species, with the S $2p_{3/2}$ BE at 162.8 eV. The present results are consistent with those of a CeO_{2-x} system prepared by sputtering with Ar^+ ions.[17] Heating to 400 K leads to an intensity decrease for sulfite (SO_3) and the appearance of another atomic species, located at 161.4 eV for S $2p_{3/2}$. This sulfur species could be assigned as a surface cerium sulfide (Ce_2O_2S) or a zirconium sulfide (Zr_2O_2S).[17,18] In addition, the number of atomic sulfur species at 162.8 eV increases because of thermal conversion. Upon heating to 500 K, the sulfite species disappears. The intensity of the sulfur species at 161.4 eV continues to increase. By 700 K, the SO_4 feature shows a decrease in intensity. At 900 K, the SO_4 species has almost completely desorbed or transformed, and the species at 161.4 eV dominates in the region of 161−164 eV.

Figure 5 summarizes the change in S 2p intensity for the total concentration of sulfur species, sulfur oxides (adsorbed SO_4 and SO_3), atomic sulfur (S), and oxy-sulfides (M_2O_2S, M= Ce or Zr), shown in the right panel of Figure 4. The total amount of sulfur present in the surface decreased with the annealing temperature. Upon SO_2 adsorption at 300 K, the intensity of sulfur oxides dominates, with the intensity for atomic S being only ∼10% of that of sulfur oxides. The signal intensity for sulfate and sulfite decreases with the annealing temperature, but the intensity for the M_2O_2S sulfide increases. The signal intensity for atomic sulfur species rises from 300 to 500 K and then decreases with annealing temperature. Around 700 K, the intensity for sulfur oxides is comparable to that of atomic sulfur and sulfides. By 900 K, the intensity for atomic S species and sulfides (about ∼60% that of sulfur oxides at 300 K) is larger than that of SO_4 and SO_3, and the total concentration of sulfur species at 900 K is about ∼65% of that at 300 K. The changing trend of sulfur-containing species with annealing temperatures implies the thermal conversion of either sulfur oxides or atomic sulfur species to sulfides and the partial desorption of sulfur oxides (probably as SO_2).

The left panel of Figure 4 shows the effect of SO_2 adsorption on the valence band features of $Ce_{0.9}Zr_{0.1}O_{1.50}(111)$ after dosing at room temperature and subsequent heating in vacuum. SO_2 dosing significantly attenuates the intensity of both the O 2p features and $Ce^{\delta+}$ states. Prior to SO_2 adsorption, in the band gap region, the main feature is the $Ce^{\delta+}$-derived states with an intensity comparable to that of the O 2p states. The decrease of ∼40% in the $Ce^{\delta+}$ intensity upon SO_2 adsorption suggests the partial oxidation of the surface. Heating from 400 to 900 K results in minor changes in the line shape and the intensity of the valence band. The desorption and/or decomposition of sulfates and sulfites and the formation of the sulfide do not result in a significant reoxidation of the ceria−zirconia surface, implying the formation of a Ce^{3+}-type sulfide such as Ce_2O_2S, which is a stable compound.[18,26]

Figure 6 displays the effects of SO_2 exposure on the Zr 3d core levels of the $Ce_{0.9}Zr_{0.1}O_{1.50}(111)$ surface used in the experiments of Figure 4. Prior to SO_2 exposure, the Zr $3d_{5/2}$ peak is located at ∼183.0 eV. Upon SO_2 adsorption, the Zr $3d_{5/2}$ BE is shifted to a lower value, ∼182.9 eV, and the intensity of Zr 3d is decreased by ∼40%. Annealing at 400 and 500 K does not lead to observable changes in the BE value. At 700 K, the BE is located at 182.7 eV. Heating up to 900 K continues to shift the Zr $3d_{5/2}$ peak to lower BE, ∼182.6 eV. The intensity change for Zr 3d is shown at the bottom of Figure 6. From 300 to 900 K, the Zr 3d intensity gradually increases. The shift of the BE values points to a change in the chemical environment of the Zr atoms. It may be a consequence of direct bonding with sulfur species (probably M_2O_2S formation) or changes in the Ce−O−Zr interactions induced by sulfur.

3.2. SO_2 Interaction with $Ce_{0.7}Zr_{0.3}O_{2-x}$(111). We have also studied SO_2 adsorption and reaction on other ceria−zirconia substrates such as $Ce_{0.7}Zr_{0.3}O_{1.95}(111)$ and $Ce_{0.7}Zr_{0.3}O_{1.50}(111)$

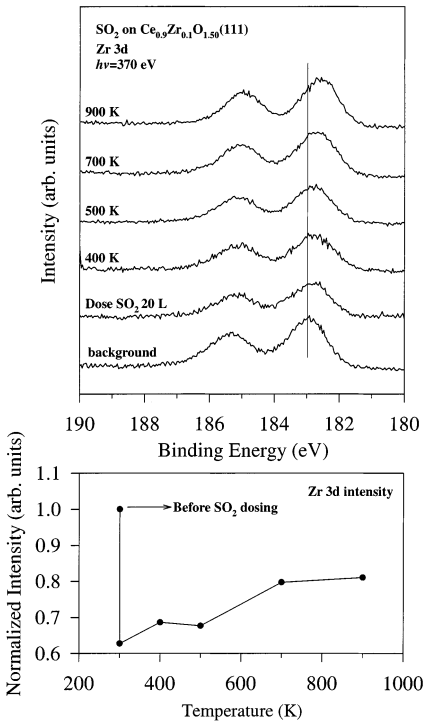

Figure 6. Zr 3d core-level spectra ($h\nu = 370$ eV) and the change in Zr 3d intensity for SO_2 adsorption and subsequent annealing on the $Ce_{0.9}$ $Zr_{0.1}O_{1.50}(111)$ surface of Figure 4.

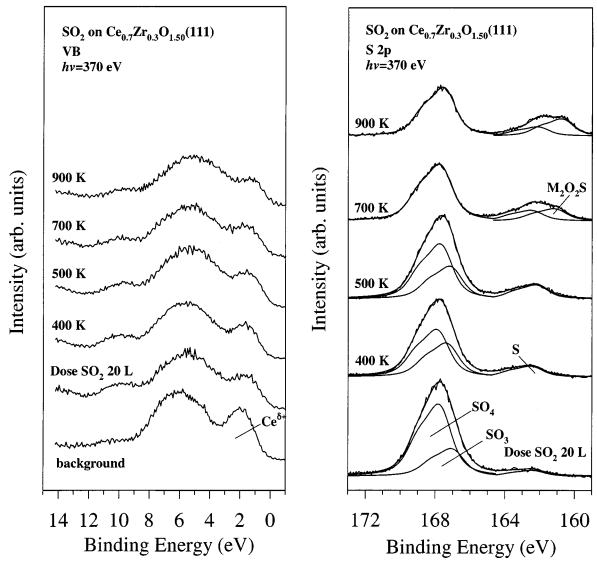

Figure 7. Effects of SO_2 adsorption and subsequent annealing on the valence band (left panel, $h\nu = 370$ eV) and corresponding S 2p spectra (right panel, $h\nu = 370$ eV) of a highly defective $Ce_{0.7}Zr_{0.3}O_{1.50}(111)$ surface containing $Ce^{\delta+}$ ($\delta \leq 3$). M = Ce or Zr.

to explore the product dependence on the population of oxygen vacancies and Ce/Zr ratio. The photoemission results (data not shown) of SO_2 adsorption on a slightly defective $Ce_{0.7}Zr_{0.3}O_{1.95}$-(111) surface point to the formation of SO_4/SO_3 species as seen for $Ce_{0.9}Zr_{0.1}O_{1.95}(111)$ above, but the large content of Zr enhanced the thermal stability of the SO_4/SO_3 groups at high temperatures. The left panel of Figure 7 shows the valence features for a $Ce_{0.7}Zr_{0.3}O_{1.50}(111)$ surface upon SO_2 adsorption and reaction. The intensity of $Ce^{\delta+}$ states for $Ce_{0.7}Zr_{0.3}O_{1.50}$-(111) is less than that of $Ce_{0.9}Zr_{0.1}O_{1.50}(111)$, as expected from the changing Ce/Zr ratio. Upon SO_2 adsorption, the intensities of the O 2p features and $Ce^{\delta+}$ states are reduced. Annealing

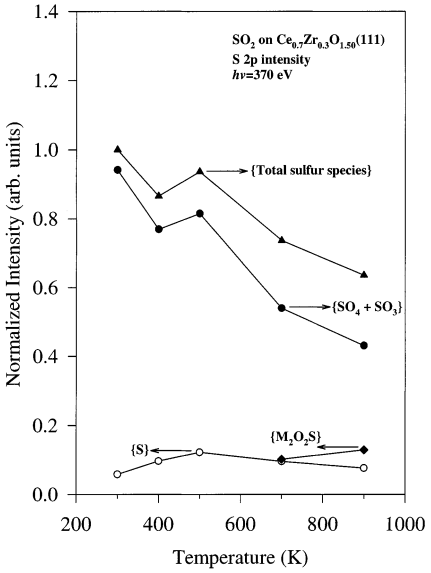

Figure 8. Change in S 2p intensity for the total concentration of sulfur species, sulfur oxides (SO_4 and SO_3), atomic sulfur, and oxy-sulfides (M_2O_2S, M = Ce or Zr) on $Ce_{0.7}Zr_{0.3}O_{1.50}(111)$ (see Figure 7) as a function of annealing temperature.

from 300 to 900 K does not lead to significant changes in the valence features. The right-side panel in Figure 7 displays the reaction and evolution of sulfur-containing species. The solid line passing through the data indicates the total intensity obtained during curve fitting.[25] Upon dosing at 300 K, the line shape indicates that at least two species produce the photoemission features above 165 eV. These two species could be sulfate and sulfite (see above), with the S $2p_{3/2}$ components located at 167.9 and 167.2 eV, respectively. A relatively small number of atomic sulfur species are seen at 162.3 eV. Annealing to 400 K leads to an increase in the intensity of atomic sulfur species and a decrease in sulfur oxides. By 700 K, SO_3 species are either desorbed or transformed, and sulfides are seen at 161.0 eV. At 900 K, SO_4, atomic sulfur species, and sulfides coexist on the surface.

Figure 8 displays the intensity change of sulfur-containing species with the annealing temperature. The total coverage of sulfur species is decreased with the annealing temperature. At 300 K, the intensity of atomic sulfur species is about 5% of that of sulfur oxides. With the rise in temperature, the intensity for SO_4 and SO_3 is decreased, and the intensity for sulfides is increased from 700 to 900 K. The signal intensity for atomic sulfur increases with annealing temperature up to 500 K and then decreases with annealing. Unlike the case for the $Ce_{0.9}$-$Zr_{0.1}O_{1.50}(111)$ sample, by 900 K, the intensity of atomic sulfur and sulfides is still only ~50% of that for sulfur oxides, and the total amount of sulfur at 900 K is about ~65% of that at 300 K. The general trend of Figure 8 is similar to that of Figure 5. On the basis of the results of Figures 3, 5, and 8, it is clear that the concentration of atomic sulfur species and sulfides depends on the defect population and the Zr/Ce ratio. An increase in the Zr/Ce ratio enhances the stability of the SO_4/SO_3 species.

Figure 9 displays the changes in the Zr 3d core-level with the adsorption and reaction of SO_2 on the $Ce_{0.7}Zr_{0.3}O_{1.5}(111)$ surface. Prior to SO_2 exposure the Zr $3d_{5/2}$ peak is located at ~182.7 eV. Upon SO_2 adsorption, the Zr $3d_{5/2}$ BE is shifted to a lower value, ~182.4 eV, and the intensity of the Zr $3d_{5/2}$ peak is decreased by ~30%. Annealing at 400 and 700 K does not lead to observable changes in the BE values. Heating up to 900

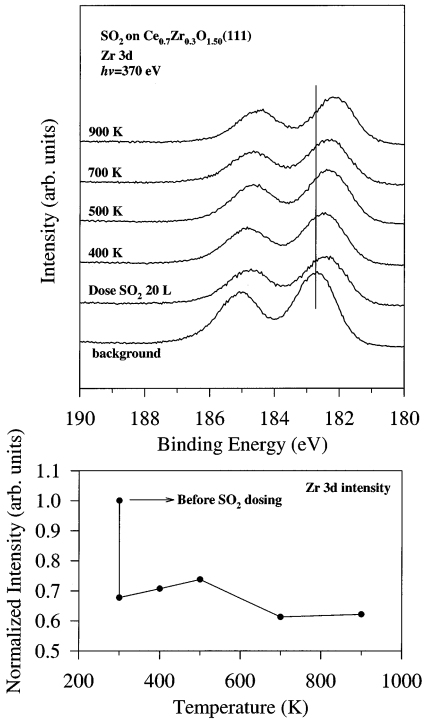

Figure 9. Zr 3d core-level spectra ($h\nu = 370$ eV) and the change in Zr 3d intensity for SO_2 adsorption and subsequent annealing on the $Ce_{0.7}$ $Zr_{0.3}O_{1.50}(111)$ surface of Figure 7.

K continues to shift the Zr $3d_{5/2}$ peak to lower BE, ~182.1 eV. As mentioned above, this BE shift may be due to the formation of bonds between Zr and sulfur-containing species or an adsorbate-induced change in the Ce−O−Zr interactions. The intensity change for Zr 3d is shown in the bottom panel of Figure 9. From 300 to 500 K, the Zr 3d intensity gradually increases. From 500 to 900 K, the intensity is slightly decreased. From this and the BE shifts, it seems that the sulfate species are directly bonded and cover the Zr atom at high temperature.

4. Discussion

In general, the addition of zirconia to ceria, which operates as a crucial promoter in three-way catalytic converters for emission control in automobiles, increases the oxide thermal stability and facilitates catalyst operations over a wide range of temperatures and operating conditions.[5,6] The increased activity of ceria−zirconia can be correlated to its higher reducibility and to the enhanced mobility of oxygen anions.[5,6] Pure ceria has been reported to be highly susceptible to deactivation by sulfur species, and sulfate is believed to be responsible for the deactivation activity.[14−16] In addition to sulfates, other species such as sulfites and Ce_2O_2S are observed for SO_2 on ceria[18] and ceria-supported Pd catalysts.[27] The complexity of the chemistry involving a number of sulfur-containing compounds is attributed to the Ce−O−S phase diagram.[27] However, fundamental information involving the reaction channels and the intermediates in the deactivation process of ceria−zirconia has not been fully examined.

The present results suggest that sulfate is the only species formed upon SO_2 adsorption at 300 K on nearly defect-free surfaces such as $Ce_{0.9}Zr_{0.1}O_{1.95}(111)$ and $Ce_{0.7}Zr_{0.3}O_{1.95}(111)$. Figure 10 shows the structure of an ideal $Ce_{1-x}Zr_xO_2(111)$ surface. The top layer consists of an O atom, but within this layer there are holes that expose the Ce or Zr cations in the second layer. For sulfate formation, the reaction pathway is facilitated by the lattice oxygen from ceria−zirconia through

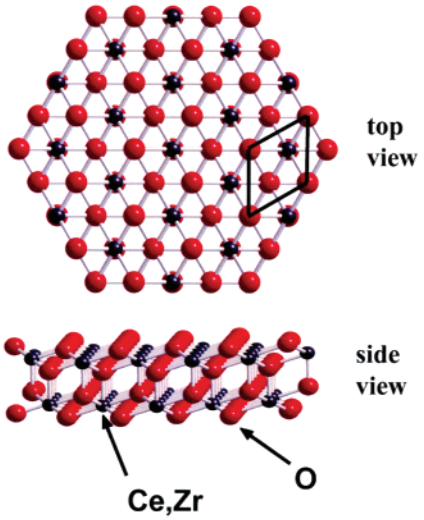

Figure 10. Top and side views of an oxygen-terminated $Ce_{1-x}Zr_xO_2(111)$ surface. The red spheres represent O atoms, and the black spheres correspond to Ce or Zr atoms in a solid solution.

an exothermic reaction such as[17,18]

$$CeO_2(s) + 4SO_2(g) \rightarrow 2SO(g) + Ce(SO_4)_2(s) \qquad (1)$$

In this reaction, the Ce^{4+} cations play a secondary or indirect role in the interaction with SO_2. It has been reported that for $Ce_{0.9}Zr_{0.1}O_2$ and $Ce_{0.7}Zr_{0.3}O_2$ systems the Zr ions substitutionally replace Ce ions within the cubic fluorite lattice structure of CeO_2.[20,21] As a consequence, an alternate adsorption pathway could also involve the Zr^{4+} cations through the following reaction (M = Ce or Zr):

$$MO_2(s) + 4SO_2(g) \rightarrow 2SO(g) + M(SO_4)_2(s) \qquad (2)$$

In a parallel reaction channel, SO_2 could be oxidized by surface oxygen anions to form sulfate without producing SO:[17,18]

$$SO_2(g) + 2O \rightarrow SO_4(s) \qquad (3)$$

The $Ce_{1-x}Zr_xO_2(111)$ thin films used in the present study possess a pure and single-crystalline phase, and these (111) surfaces are oxygen-terminated.[20,28−30] It is well known that the catalytic activity and oxygen-transport properties of ceria are structure-sensitive.[31,32] Generally, thermal annealing produces point defects in the bulk and/or surface without generating rough morphology as observed from ion sputtering.[28−30] Our previous studies[17] show that on fully oxidized CeO_2 surfaces SO_4 is formed, as evidenced by both XANES and XPS. Thus, the O centers are very efficient for oxidizing and trapping SO_2. The present results also show that for mixed oxides with a small fraction of oxygen vacancies the chemistry of SO_2 on $Ce_{0.9}Zr_{0.1}O_{1.95}(111)$ and $Ce_{0.7}Zr_{0.3}O_{1.95}(111)$ is similar to that on fully oxidized CeO_2 except that the SO_4 decomposition temperature is different from those of previous studies.[17−19]

For defect-rich surfaces such as $Ce_{0.9}Zr_{0.1}O_{1.50}(111)$ and $Ce_{0.7}Zr_{0.3}O_{1.50}$ (111) at 300 K, in addition to sulfates and atomic sulfur species, another sulfur species is observed. Previous studies demonstrate that the introduction of O vacancies on pure ceria thin films or powders[15,17,18] favors the formation of sulfite at the expense of sulfate. This reaction pathway directly involves chemisorption via a lattice oxygen anion (O) to form sulfite, or in terms of molecularly adsorbed SO_2,[18,19]

$$SO_2(g) + O \rightarrow SO_3(s) \qquad (4)$$

Recent theoretical studies show that oxygen vacancies in $TiO_2(110)$[33] and $MgO(100)$[34] play an important role in adsorbing and dissociating the SO_2 molecule. The extra electrons around the oxygen vacancies are in part transferred to the LUMO of the SO_2 molecule.[33,34] This charge transfer facilitates dissociation because this orbital is S−O antibonding.[35,36] Fully oxidized metal cations are not able to carry out such charge transfer.[33,34] The relative concentration for sulfur-containing species measured in our photoemission studies depends on the defect (or $Ce^{\delta+}$) concentration of the samples. The defective surfaces probably act a better sorbent for SO_2 by supplying multiple adsorption sites and reaction channels.

On the basis of the fact that the formation of $Ce_2(SO_4)_3$ is thermodynamically favored over $Ce(SO_4)_2$ and $Zr(SO_4)_2$,[37] we propose the following mechanism for SO_2 adsorption and decomposition on highly defective ceria−zirconia surfaces:

$$5SO_2(g) + M_2O_3(s) \rightarrow M_2(SO_4)_3(s) + SO(g) + S(s) \quad (5)$$

Upon annealing, the $M_2(SO_4)_3$ species is transformed to M_2O_2S via the following reaction:

$$M_2(SO_4)_3(s) \rightarrow M_2O_2S(s) + 2SO_2(g) + 3O_2(g) \quad (6)$$

In another approach, $M(SO_4)_2$ is reduced to M_2O_2S by

$$2M(SO_4)_2(s) \rightarrow M_2O_2S(s) + 3SO_2(g) + 4O_2(g) \quad (7)$$

Because no significant reoxidation of the ceria−zirconia was observed, reaction channels 6 and 7 could take place concurrently.

The negative shifts of the Zr 3d BE and the attenuation of Zr 3d intensity (shown in Figures 6 and 9) upon SO_2 adsorption suggest the participation of Zr cations in the surface chemistry of the SO_x species. Sulfates such as $M(SO_4)_2$ could be formed at low temperatures, with M_2O_2S present at high temperatures. This would imply a change in the formal oxidation state of Zr from +4 to +3, which is consistent with the core-level shifts observed in Figures 6 and 9. According to our results, zirconia does not play the same role in the chemistry of SO_2 under UHV conditions that the $Ce^{\delta+}$ defects do. Thus, whereas $Ce^{\delta+}$ states favor the decomposition of SO_x groups, a large content of Zr enhances the thermal stability of SO_x species. This could affect the capacity of the oxide to release and storage oxygen.[2,16] It is not clear how the Zr cations enhance the thermal stability of SO_x species on the cerium oxide. Our previous studies[8,9] demonstrate that for both single-crystal thin films and nanoparticles the incorporation of zirconia into ceria leads to structural and electronic perturbations that can modify the chemical properties of the oxide substrate.

5. Summary and Conclusions

The interaction of SO_2 with ceria−zirconia model catalysts was studied using high-resolution synchrotron-based X-ray photoelectron spectroscopy (XPS). Epitaxial $Ce_{1-x}Zr_xO_2(111)$ ($x = 0.1$ and 0.3) thin films (500−700 Å in thickness) were grown by oxygen-plasma-assisted molecular beam epitaxy on single-crystal Y-stabilized $ZrO_2(111)$. Slightly defective surfaces were achieved by vacuum annealing at 900 K, and highly defective surfaces with O vacancies were obtained by 1.5-keV Ne^+ sputtering. On the slightly defective $Ce_{0.9}Zr_{0.1}O_{1.95}(111)$ and $Ce_{0.7}Zr_{0.3}O_{1.95}(111)$ surfaces, the only products upon SO_2 adsorption at 300 K are the SO_4/SO_3 species, which gradually desorb from the surface between 300 and 900 K. SO_2 adsorption on the heavily reduced surfaces results in different behavior. A complex set of compounds is observed during adsorption and thermal conversion processes. The $Ce^{\delta+}$ states ($\delta \leq 3$) play a dominant role in the adsorption of SO_2 and cleavage of S−O bonds. The relative concentration of sulfur-derived adsorbates depends on the defect concentration: the higher the $Ce^{\delta+}$ concentration, the larger the amount of formed atomic S. On $Ce_{0.9}Zr_{0.1}O_{1.50}(111)$ and $Ce_{0.7}Zr_{0.3}O_{1.50}(111)$ surfaces, sulfate, sulfite, and atomic sulfur species coexist at 300 K. The Zr cations increase the stability of the SO_4/SO_3 groups on the oxide surface. Thermal annealing (for $Ce_{0.9}$ $Zr_{0.1}O_{1.50}(111)$, >400 K; for $Ce_{0.7}Zr_{0.3}O_{1.50}(111)$, >700 K) leads to the formation of oxy-sulfides (M_2O_2S, M = Ce or Zr), which are converted from either sulfate or sulfite. The formation of the oxy-sulfides produces a substantial shift in the Zr 3d core levels.

Acknowledgment. This research was primarily carried out at Brookhaven National Laboratory and was supported by the U.S. Department of Energy (DOE), Division of Chemical Sciences, under contract DE-AC02-98CH10886. The NSLS is supported by the Division of Materials and Chemical Sciences of DOE. A portion of the work was performed in the Environmental Molecular Sciences Laboratory (EMSL), a national scientific user facility located at Pacific Northwest National Laboratory and supported by the DOE Office of Biological and Environmental Research. C.H.F.P. acknowledges the funding for his work from the DOE, Office of Basic Energy Sciences, Division of Chemical Sciences.

References and Notes

(1) Stern, A. C.; Boubel, R. W.; Turner, D. B.; Fox, D. L. *Fundamentals of Air Pollution*, 2nd ed.: Academic Press: Orlando, FL, 1984.

(2) (a) Trovarelli, A. *Catal. Rev. Sci. Eng.* **1996**, *38*, 439. (b) Rodriguez, J. A.; Wang, X.; Hanson, J. C.; Liu, G.; Iglesias-Juez, A.; Fernández-García, M. *J. Chem. Phys.* **2003**, *119*, 5659. (c) Rodriguez, J. A. *Catal. Today* **2003**, *85*, 177.

(3) Taylor, K. C. *Catal. Rev. Sci. Eng.* **1995**, *35*, 457.

(4) *Basic Research Needs for Vehicles of the Future*; Eisenberger, P. M., Ed; Princeton Materials Institute: Princeton, NJ, 1995.

(5) Putna, E. S.; Bunluesin, T.; Fan, X. L.; Gorte, R. J.; Vohs, J. M.; Lakis, R. E.; Egami, T. *Catal. Today* **1999**, *50*, 343.

(6) Fornasiero, P.; Fonda, E.; Di Monte, R.; Vlaic, G.; Kašpar, J.; Graziani, M. *J. Catal.* **1999**, *187*, 177.

(7) Mamontov, E.; Egami, T.; Brezny, R.; Koranne, M.; Tyagi, S. *J. Phys. Chem. B* **2000**, *104*, 11110.

(8) Liu, G.; Rodriguez, J. A.; Hrbek, J.; Dvorak, J.; Peden, C. H. F. *J. Phys. Chem. B* **2001**, *105*, 7762.

(9) Rodriguez, J. A.; Hanson, J. C.; Kim, J.-Y.; Liu, G.; Iglesias-Juez, A.; Fernández-García, M. *J. Phys. Chem. B* **2003**, *107*, 3535.

(10) Rodriguez, J. A.; Hrbek, J. *Acc. Chem. Res.* **1999**, *32*, 719.

(11) Thomas, J. M.; Thomas, W. J. *Principles and Practice of Heterogeneous Catalysis*; VCH: New York, 1997.

(12) Pieplu, A.; Saur, O.; Lavalley, J.-C.; Legendre, O.; Nedez, C. *Catal. Rev. Sci. Eng.* **1998**, *40*, 409.

(13) Beck, D. D.; Sommers, J. W.; DiMaggio, C. L. *Appl. Catal. B* **1997**, *11*, 273.

(14) (a) Truex, T. J. *Soc. Automot. Eng. SP* **1999**, *1459*, 173. (b) Daturi, M.; Finocchio, E.; Binet, C.; Lavalley, J. C.; Fally, F.; Perrichon, V.; Vidal, H.; Hickey, N.; Kaspar, J. *J. Phys. Chem. B* **2000**, *104*, 9186.

(15) Waqif, W.; Bazin, P.; Saur, O.; Lavalley, J. C.; Balanchard, G.; Touret, O. *Appl. Catal. B* **1997**, *11*, 193.

(16) Boaro, M.; de Leitenburg, C.; Dolcetti, G.; Trovarelli, A.; Graziani, M. *Top. Catal.* **2001**, *16/17*, 1.

(17) Rodriguez, J. A.; Jirsak, T.; Freitag, A.; Hanson, J. C.; Larese, J. Z.; Chaturvedi, S. *Catal. Lett.* **1999**, *62*, 113.

(18) Ferrizz, R. M.; Gorte, R. J.; Vohs, J. M. *Catal. Lett.* **2002**, *82*, 123.

(19) Overbury, S. H.; Mullins, D. R.; Huntley, D. R.; Kundakovic, Lj. *J. Phys. Chem. B* **1999**, *103*, 11308.

(20) Kim, Y. J.; Thevuthasan, S.; Shutthananadan, V.; Perkins, C. L.; McCready, D. E.; Herman, G. S.; Gao, Y.; Tran, T. T.; Chambers, S. A.; Peden, C. H. F. *J. Electron Spectrosc. Relat. Phenom.* **2002**, *126*, 177.

(21) Shutthanandan, V.; Thevuthasan, S.; Kim, Y. J.; Peden, C. H. F. *Mater. Res. Soc. Symp. Proc.* **2001**, *654*, AA2.6/1.

(22) Mullins, D. R.; Radulovic, P. V.; Overbury, S. H. *Surf. Sci*. **1999**, *429*, 186.
(23) Mullins, D. R.; Overbury, S. H.; Huntley, D. R. *Surf. Sci.* **1998**, *409*, 307.
(24) Burroughs, P.; Hamnett, A.; Orchard, A. F.; Thornton, G. *J. Chem. Soc., Dalton Trans.* **1976**, *17*, 1686.
(25) (a) Liu, G.; Rodriguez, J. A.; Hrbek, J.; Long, B. T.; Chen, D. A. *J. Mol. Catal. A* **2003**, *202*, 215. (b) Hrbek, J.; Li, S. Y.; Rodriguez, J. A.; van Campen, D. G.; Huang, H. H.; Xu, G. Q. *Chem. Phys. Lett.* **1997**, *267*, 65. (c) The intensity ratio within the S 2p doublet was fixed as 1:2 with a constant distance (1.2 eV) between the doublet components. The fitting function was a Doniac-Sunjic natural line shape convoluted with Gaussian and Lorentzian functions. The Gaussian width, Lorentzian width, and Doniac-Sunjic asymmetry parameter were allowed to vary in the fits but were constrained to be the same for all of the components in a given spectrum.
(26) Kay, D. A. R.; Wilson, W. G.; Jalan, V. *J. Alloys Comput.* **1993**, *192*, 11.
(27) Luo, T.; Vohs, J. M.; Gorte, R. J. *J. Catal.* **2002**, *210*, 397.
(28) Fukui, K.-i.; Namai, Y.; Iwasawa, Y. *Appl. Surf. Sci.* **2002**, *188*, 252.
(29) Nörenberg, H.; Briggs, G. A. D. *Surf. Sci.* **1999**, *424*, L352.
(30) Nörenberg, H.; Briggs, G. A. D. *Phys. Rev. Lett.* **1997**, *79*, 4222.
(31) Ferrizz, R. M.; Egami, T.; Vohs, J. M. *Surf. Sci.* **2000**, *465*, 127.
(32) Stubenrauch, J.; Vohs, J. M. *J. Catal.* **1996**, *159*, 50.
(33) Rodriguez, J. A.; Liu, G.; Jirsak, T.; Hrbek, J.; Chang, Z.; Dvorak, J.; Maiti, A. *J. Am. Chem. Soc.* **2002**, *124*, 5242.
(34) Rodriguez, J. A.; Jirsak, T.; González, L.; Evans, J.; Pérez, M.; Maiti, A. *J. Chem. Phys.* **2001**, *115*, 10914.
(35) Rodriguez, J. A. *Surf. Sci.* **1990**, *226*, 101.
(36) Rodriguez, J. A.; Ricart, J. M.; Clotet, A.; Illas, F. *J. Chem. Phys.* **2001**, *115*, 454.
(37) *Lange's Handbook of Chemistry*, 13th ed.; Dean, J. A., Ed.; McGraw-Hill: New York, 1985.